



## High precision $\delta^{18}\text{O}$ measurements of atmospheric dioxygen using optical-feedback cavity-enhanced absorption spectroscopy (OF-CEAS)

Clément Piel<sup>1</sup>, Daniele Romanini<sup>2</sup>, Morgane Farradèche<sup>3</sup>, Justin Chaillot<sup>3</sup>, Clémence Paul<sup>3</sup>, Nicolas Bienville<sup>3</sup>, Thomas Lauwers<sup>3</sup>, Joana Sauze<sup>1</sup>, Kevin Jaulin<sup>4</sup>, Frédéric Prié<sup>3</sup>, Amaëlle Landais<sup>3</sup>

5 <sup>1</sup> Ecotron Européen de Montpellier (UAR 3248), Centre National de la Recherche Scientifique (CNRS), Université de Montpellier, Campus Baillarguet, Montferrier-sur-Lez, France

<sup>2</sup> Laboratoire Interdisciplinaire de Physique, Univ Grenoble Alpes, CNRS/UGA, Saint-Martin-d'Hères, France

<sup>3</sup> Laboratoire des Sciences du Climat et de l'Environnement, LSCE - IPSL, CEA-CNRS-UVSQ, Université Paris-Saclay, 91191 Gif-sur-Yvette, France

10 <sup>4</sup> AP2E, 240, rue Louis de Broglie, Les Méridiens Bâtiment A, CS90537, F-13593 Aix-en-Provence, FRANCE

Correspondence: Clément Piel (clement.piel@cnrs.fr)

### **Short summary**

This paper introduces a new optical gas analyzer based on the Optical-Feedback Cavity-Enhanced Absorption Spectroscopy technique (OF-CEAS) enabling high temporal resolution and high precision  
15 measurement of  $\delta^{18}\text{O}$  and concentration of atmospheric  $\text{O}_2$ . The results underscore the good agreement with dual inlet IRMS measurements and the ability of the instrument to monitor biological processes.

### **Abstract**

Atmospheric dioxygen concentration and isotopic composition are closely linked to the carbon cycle  
20 through anthropic  $\text{CO}_2$  emissions and biological processes such as photosynthesis and respiration. Measurement of isotopic ratio of atmospheric dioxygen, trapped in ice core bubbles, bring information about past variation in the hydrological cycle at low latitudes, as well as past productivity. Currently, the interpretation of those variations could be drastically improved with a better (*i.e.* quantitative) knowledge of the oxygen fractionation that occur during photosynthesis and respiration  
25 processes. This could be achieved, for example, during experiment using closed- biological chambers.



In order to estimate the fractionation coefficient with a good precision, one of the principal limitations is the need of high frequency on-line measurements of  $\delta^{18}\text{O}$  of  $\text{O}_2$  and  $\text{O}_2$  concentration. To address this issue, we developed a new instrument, based on the OF-CEAS (Optical-Feedback Cavity-Enhanced Absorption Spectroscopy) technique, enabling high temporal resolution and continuous  
30 measurements of dioxygen concentration as well as  $\delta^{18}\text{O}$  of  $\text{O}_2$ , both simultaneously. Minimum of Allan deviation occurred between 10 and 20 minutes while precision reached 0.002 % for  $\text{O}_2$  concentration and 0.06 ‰ for  $\delta^{18}\text{O}$  of  $\text{O}_2$ , which correspond to the optimal integration time and analytical precision before drift start degrading the measurements. While humidity did not affect much the measured values,  $\text{O}_2$  concentration had an influence on  $\delta^{18}\text{O}$  of  $\text{O}_2$ , which should hence be  
35 quantified. To ensure good quality of  $\text{O}_2$  concentration and  $\delta^{18}\text{O}$  of  $\text{O}_2$  measurements we eventually proposed to measure calibration standard every 20 minutes.

## **1. Introduction**

Dioxygen is the second most important constituent of the atmosphere and the evolution of its atmospheric concentration is closely related to the evolution of the carbon cycle through fossil fuel  
40 combustion and biosphere processes (respiration and photosynthesis). The atmospheric dioxygen concentration has been shown to decrease by 0.7 % over the last 800 ka probably because of changes of organic carbon burial and oxidation rates with a stabilizing effect of silicate weathering (Stolper et al., 2016). On shorter timescales, the dioxygen concentration is showing clear seasonal variations anticorrelated with atmospheric  $\text{CO}_2$  concentration, the combination of both  $\text{O}_2$  and  $\text{CO}_2$   
45 concentrations enabling to document the variability of the marine and terrestrial biosphere productivity through calculation of the atmospheric potential oxygen (e.g. Keeling and Shertz, 1992; Stephens et al., 1998; Keeling and Manning, 2014; Goto et al., 2017).

The isotopic composition of atmospheric dioxygen, expressed as  $\delta^{18}\text{O}$  of  $\text{O}_2$  or  $\delta^{18}\text{O}_{\text{atm}}$ , exhibits variations at the orbital (10,000 years) and millennial scale (Severinghaus et al., 2009; Landais et al.,  
50 2010) but no appreciable variation at the seasonal scale has been evidenced. Past  $\delta^{18}\text{O}_{\text{atm}}$  variability has been linked to variations in low latitude water cycle and possibly to the variability of the relative proportions of terrestrial and marine productivity (Bender et al., 1994; Luz and Barkan, 2011; Extier et al., 2018). Still, evaluating the relative importance of these two contributions remains difficult since it relies on fractionation factors associated with the biological processes consuming and producing  
55 oxygen. These fractionation factors have only been determined for a small number of species and often at the micro-organism scale.



Combining measurements of  $\delta^{17}\text{O}$  and  $\delta^{18}\text{O}$  of  $\text{O}_2$  permits to have access to gross primary production and is largely used for this purpose in the ocean in combination with the  $\text{O}_2/\text{Ar}$  ratio (Luz and Barkan, 2000; Stanley et al, 2010; Jurikova et al, 2022). In addition, when measuring  $\Delta^{17}\text{O}$  of  $\text{O}_2$  in old air  
60 trapped in ice cores, we have access to the past variability of the global biosphere productivity although with large uncertainties (Luz et al., 1999; Blunier et al., 2002; Brandon et al., 2020; Yang et al., 2022). Part of this limitation is again linked to our poor knowledge of the isotopic fractionation factors during the biological processes.

In order to progress on the quantitative determination of the oxygen fractionation factors in the  
65 biosphere, a good approach is to work on closed biological chambers where plants grow in controlled conditions. This approach was already applied in previous studies, mostly at the micro-organism scale with regular sampling of air from the biological set-up (Guy et al., 1993; Helman et al., 2005; Stolper et al., 2018). At a larger scale such as for a macroscopic study on a terrarium the duration of the experiment needs to be larger to have a quantified signal (Luz et al., 1999).

70 One of the main limitations when working on the experimental determination of the fractionation factors is that we need numerous measurements of  $\delta^{18}\text{O}$  of  $\text{O}_2$  and  $\text{O}_2$  concentration to make a precise determination (Paul et al., 2023). However, sampling air from the chamber at high resolution is not convenient since it implies to reduce the quantity of atmospheric air in the biological chamber.

Development of continuous measurements of dioxygen concentration has permitted to improve the  
75 monitoring of atmospheric dioxygen concentration in parallel with greenhouse gases. These methods use different techniques such as fuel cell analyzer (Goto et al., 2013) or gas chromatography coupled with a thermal conductivity detector (Tohjima, 2000). More recently, Berhanu et al. (2019) developed an analyzer based on the CRDS (Cavity-Ring-Down Spectroscopy) technique which is able to measure the concentration of atmospheric dioxygen with high precision (standard error of 1 ppm over 1 minute  
80 measurement) on one mode as well as the isotopic composition of dioxygen with a 10 ppm standard error) on a second mode. However,  $\delta^{18}\text{O}$  of  $\text{O}_2$  and  $\text{O}_2$  concentrations are not measured on the same mode and so not at the same time.

We present here a new instrument based on the OF-CEAS (Optical-Feedback Cavity-Enhanced Absorption Spectroscopy) technique, able to measure the atmospheric  $\text{O}_2$  concentration and  $\delta^{18}\text{O}$  of  
85  $\text{O}_2$  in parallel. After a presentation of the instrumental design, we discuss the performances of the instrument as well as the influences of humidity on the determination of  $\text{O}_2$  concentration and isotopic composition and  $\text{O}_2$  concentration on  $\delta^{18}\text{O}$  of  $\text{O}_2$ . Based on our tests, we propose a sequence for

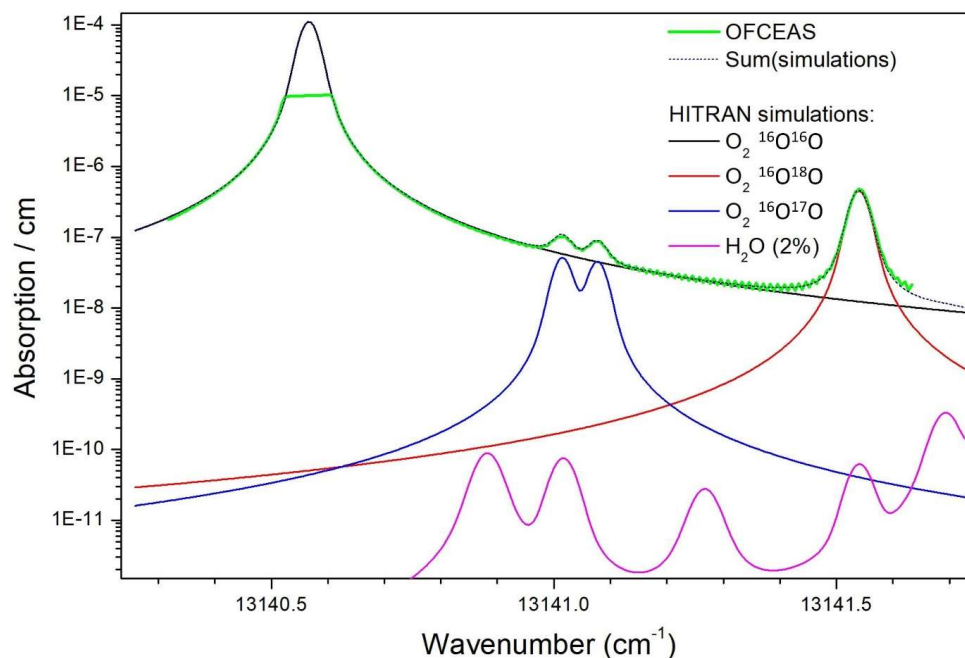


calibration of the instrument during series of measurements. This sequence is then used to compare  
the performance of this instrument to a classical IRMS for measurements of  $\delta^{18}\text{O}$  of  $\text{O}_2$  and  $\text{O}_2$   
90 concentration.

## **2. Material and methods**

### **2.1 Instrument description**

We present here a new analyzer for  $\text{O}_2$  based on the high sensitivity absorption spectroscopy  
technique OF-CEAS. This technique is based on a high finesse optical cavity and is analogous to the  
95 well-known Cavity-Ring-Down Spectroscopy. It was first described in (Morville et al., 2005) (see also  
(Morville et al., 2014) and since then successfully exploited in different laboratories and field  
applications . In addition, the simple and compact optical layout of OF-CEAS led to the development  
of robust commercial devices [[www.AP2E.com](http://www.AP2E.com)]. The instrument used in this study is based on an AP2E  
analyzer customized to satisfy some specific demands. To our knowledge this is the first OF-CEAS  
100 implementation using a DFB diode laser in the visible range, the operating wavelength of the DFB  
(Distributed Feed-Back) diode laser optical source targets a specific region of the dioxygen absorption  
band around 760 nm. This so-called “A” band is the strongest absorption band of this molecule in the  
visible and infrared spectral range, even though it is still a relatively weak “forbidden” magnetic-dipole  
transition. In this spectral region, several weak lines of the  $^{18}\text{O}$ - $^{16}\text{O}$  and  $^{17}\text{O}$ - $^{16}\text{O}$  isotopologues are  
105 present near-by strong lines of the main  $^{16}\text{O}$ - $^{16}\text{O}$  isotopologue. The specific spectral window chosen  
for our analyzer, which can be covered by a single current-driven laser frequency scan, is displayed in  
Figure 1. A second novelty of this instrument is the presence of a saturated absorption line in the  
measured absorption spectrum, as visible in the figure and further discussed below.



110

Figure 1: Air absorption spectrum from the instrument (green) superposed with HITRAN2021 simulation (black dotted) which results as the sum of absorption from the main O<sub>2</sub> isotopologues and the <sup>18</sup>O and <sup>17</sup>O varieties (respectively in red and blue). Simulated water vapor absorption for a 2 % molar fraction is plotted to show that it can be neglected in the spectral analysis. Vertical scale is logarithmic in order to allow clearer display of weaker absorption features.

115

The analyzer is a modified prototype of a new series of AP2E devices under development at the time of this work, featuring enhanced thermal insulation and stabilization (in particular, sample cell temperature is 37 °C with mK fluctuations). This allows stable measurements on longer time scales as necessary for averaging isotopic ratios and detecting their small variations when switching among samples, in particular for isotopic ratio measurements relative to a reference sample. Since gas sample switching typically implies dead times of a few minutes, due to limited flow rates and memory effects, and since a few minutes averaging are additionally required to attain sufficient precision, the shortest time for measurement of one sample is on the range of 5 to 10 minutes. Instrumental drift, assessed by the Allan deviation as presented below, should then remain below the desired precision level over the measurement time for two samples of which one would be a reference. Smaller drift would afford duty cycle gains by flushing several samples through the analyzer before injection of one calibration sample. The chosen measurement strategy will be discussed later.

120

125



130 The most recent description of an OF-CEAS instrument close to the present one is described in  
Lechevallier et al. (2019). The main difference is the visible DFB diode laser emitting at 760 nm in place  
of the mid-infrared DFB intraband cascade laser (ICL) of that work, which actually makes this the first  
OF-CEAS instrument using a visible DFB diode laser. Obviously, optical elements are replaced with  
ones adapted to 760 nm, with a simple room-temperature Si PIN photodiode to monitor cavity  
transmission. However, no reference photodiode is installed, with a simulated ramp proficiently  
135 replacing the laser power ramp for normalization of cavity transmission signals. This setup was initially  
equipped with a Nanoplus DFB diode laser featuring a large current tuning coefficient leading to  
current noise converting to excessive frequency noise at cavity transmission, even in the presence of  
the stabilizing effect of optical feedback. To solve this problem, we replaced the laser with a slower-  
tuning Toptica DFB diode emitting at the same wavelength.

140 For this setup we obtained from Layertec cavity mirrors (1m radius of curvature) with a reflection  
coefficient as good as 0.999956, allowing for ring-down times of up to 30  $\mu$ s (with room air at the  
working pressure, from a 40 cm cavity as in Lechevallier et al. (2019). As usual the sample cell has a  
small volume (less than 20 cc) which, combined with a low sample pressure (150 mBar), results in a  
transit time of about 10 s with a sample flow of only  $\sim$ 15 sccm. Another improvement is a more  
145 accurate, stable and fast control of the sample pressure inside the measurement cell, which is also  
important for low drift. In addition, a fast response allows minimization of flow and pressure  
perturbations when switching between samples, which contributes to obtain short commutation  
times.

As previously described (Kerstel and Gianfrani, 2008) isotopic ratios may be measured by optical  
150 absorption spectroscopy by obtaining spectra containing at the same time the absorption line profiles  
of an isotopologue and its main variety. In our case we are considering the dioxygen isotopologues  
mentioned above, in particular the  $^{18}\text{O}$ - $^{16}\text{O}$  variety. A simulated absorption spectrum showing close-  
by absorption lines for the working spectral region of the instrument is plotted in Figure 1 (based on  
the well-known HITRAN spectral database) together with a real spectrum obtained from the  
155 instrument. As visible in the figure, the strong  $^{16}\text{O}$ - $^{16}\text{O}$  line is truncated at the top due to saturation of  
the absorption scale of the instrument (this point will be addressed below). The isotopic ratio is then  
obtained as the ratio of the line areas for the considered isotopologue normalized to that of the main  
isotopologue. It is straightforward to demonstrate that, under conditions of constant gas sample  
temperature and pressure, this ratio is indeed linearly proportional to the ratio of the mole fractions  
160 of these species in the sample. The isotopic ratio variation (delta value -  $\delta$  - in permil units - ‰) is then



calculated after measuring the ratio of areas of the same absorption lines for a reference sample by using the simple equation (written here for the  $^{18}\text{O}$ - $^{16}\text{O}$  case):

$$\delta^{18}\text{O} = \left( \frac{\left( \frac{A_{18}}{A_{16}} \right)_{\text{sample}}}{\left( \frac{A_{18}}{A_{16}} \right)_{\text{reference}}} - 1 \right) \times 1000$$

where  $A_{18}$  and  $A_{16}$  are the area of the absorption line for  $^{18}\text{O}$ - $^{16}\text{O}$  and  $^{16}\text{O}$ - $^{16}\text{O}$  respectively.

165 Given the low relative abundances of the  $^{18}\text{O}$ - $^{16}\text{O}$  (0.2 %) and  $^{17}\text{O}$ - $^{16}\text{O}$  (0.04 %) relative to the main isotopologue  $^{16}\text{O}$ - $^{16}\text{O}$ , the corresponding absorption lines appear much less intense, by about the abundance ratio (Figure 1). For their measurement, this actually implies that the instrument sensitivity must be high to obtain the absorption lines of these minor isotopologues with sufficient signal to noise ratio. On the other hand, the absorption signal of the main variety will be so strong as to actually  
170 exceed the dynamic range of the instrument. Indeed, the high finesse (35000) optical cavity containing the sample becomes opaque (no light transmitted) when the laser diode is tuned across the center of any of the  $^{16}\text{O}$ - $^{16}\text{O}$  lines available near-by the strongest  $^{18}\text{O}$ - $^{16}\text{O}$  and  $^{17}\text{O}$ - $^{16}\text{O}$  lines in this absorption band. This problem could be avoided by choosing weaker absorption bands at other wavelengths, but no instrument would be capable as of today of providing a sufficiently good signal for the lines of the  
175 minor isotopologues. One way to avoid this would be to use a second diode laser to address a sufficiently weak main isotopologue line lying rather far away in the same absorption band or even in another absorption band (each diode laser covers a small spectral region). However, this would double size and complexity of the experimental setup. Therefore, we decided to rely on the measured wings of the main isotopologue line in order to obtain an estimate of the absorption line area. This proved  
180 to be a good strategy given the excellent performance, comparable to those obtained by the OF-CEAS technique with non-saturated absorption lines (see for example isotopic measurements on  $\text{H}_2\text{O}$ , Landsberg et al., 2014). Even if this estimate may be affected by a multiplicative form factor, this same factor will affect measurements of the reference sample and cancel out in the above equation. The situation is particularly favorable for measurement of samples presenting small concentration  
185 variations from the target species, as is the case here for dioxygen in atmospheric air varying from about 18 to 23 % in biological experiments.

In order to obtain the area of the saturated line of the main isotopologue, we exploit the fact that the data analysis software is able to “count” the cavity modes, each corresponding to a data point in the spectrum (Morville et al., 2014). This works well even though there is here a large region in the laser



190 spectral scan where points are missing. This is possible thanks to the fact that cavity modes appear  
uniformly spaced over the laser scan. In addition, we had to take care of the fact that, due to  
temperature drift, the cavity length slowly changes. As a consequence, the absolute frequency  
positions of the cavity modes changes, thus at the end the position of the data points over the  
absorption line profiles changes too. That implies that one or the other of the two modes which are  
195 on the two sides of the strong line may go above/below the threshold for being used by the spectral  
fit. Such a change of the number of datapoints in the fit causes a discontinuity in the retrieved line  
areas. In order to fix this problem, we used the position of the data points relative to the absorption  
lines to continuously adjust (at the mK level) the cavity temperature setpoint and keep the cavity  
modes at absolute fixed frequency positions. This also allows more stable retrieval of all line areas  
200 from the spectral fit, as the spectral data points keep fixed positions relative to the absorption profiles  
which are fitted by Rautian profiles. Even if the Rautian model is much better than the more widely  
used Voigt profile, it still does not perfectly describe real line profiles. Thus, a displacement of the data  
points induces small changes in the fit results (even in the absence of noise).

Over the time span of presented results (18 months), we tested two different instrument  
205 configurations. For both initial and second configurations, we finally obtained similar performances.  
The main difference between the two configurations is the high reflectivity mirrors installed on the V-  
shaped optical cavity. For the initial configuration and its corresponding set of mirrors, the cavity  
finesse was higher by about a factor 2. The cavity throughput was also higher, which induced a higher  
level of scattered light and higher level of interference fringes on the recorded spectra. The second  
210 set of mirrors, corresponding to the second configuration with lower reflectivity, had also lower  
transmission (higher absorption losses in the coatings). This tuning produced less signal on the  
photodetector at cavity output but with less parasitic fringes. In both cases the setup was carefully  
optimized in particular light traps were placed at all positions possibly causing light scatter by  
secondary light reflections. In the following we will specify which setup was used for which results  
215 which will account for somewhat varying performances.

## 2.2 Air stream selection

The air stream allowed to the instrument inlet was selected using a Valco multiposition valve (EUTF-  
SD8MWE, VICI AG, Switzerland),  $\frac{1}{8}$  PFA tubing (PFA-T2-030-100, Swagelok), and filtered using a  
Swagelok 7 $\mu$ m filter (SS-2F-7). Three gas streams, at ambient pressure, could be selected by the Valco  
220 valve: (1) synthetic mixture of O<sub>2</sub> and N<sub>2</sub> with an O<sub>2</sub> concentration similar to ambient (synthetic dry  
air, Alphagaz 2, Air Liquide France), (2) ambient atmospheric air (sampled at the inlet of the room





ventilation duct) dried with a 40 mL magnesium perchlorate filter, (3) natural dry atmospheric air cylinder enriched in oxygen (Natural Air enriched at 22.9 % O<sub>2</sub>, Air Liquide Spain) subsequently diluted with N<sub>2</sub> (Alphagaz 2, Air Liquide France) using two mass flow controllers (F200CV and F201CV, 225 Bronkhorst, The Netherlands). All the measurements took place in a temperature-controlled room, with temperature fluctuations within +/- 2 °C around setpoint.

In routine mode, humid air was dried using a 20 cm long home-made humidity trap made with 6 mm PFA tubing (Swagelok PFA-T6M-1M-30M). This trap was daily replaced. For water vapor dependency measurements, the humidity trap was removed, and a stream of synthetic air (Air Product, < 3 ppm of 230 water), with constant O<sub>2</sub> concentration and δ<sup>18</sup>O, was humidified at a constant setpoint using a vapor generator (see Leroy-Dos Santos et al., 2021 for more details) up to 9,000 ppm.

### 2.3 Isotope-ratio mass spectrometry (IRMS) measurements

IRMS analyses were used as a reference method to validate measurement achieved with OF-CEAS technique. Samples of air were punctually collected in 5 ml glass flasks to be analyzed through IRMS. 235 Operation of the automated sampling system is detailed in Paul et al (submitted). Briefly, air from a closed chamber system was circulating through the instrument and the flask for 30 min. Then the flask was automatically isolated thanks to two valves and collected to be analyzed. Results from the flask and the 30 min data acquisition were, in the end, compared.

Flasks were analyzed for δ<sup>18</sup>O of O<sub>2</sub> and δO<sub>2</sub>/Ar. δO<sub>2</sub>/Ar can be converted into O<sub>2</sub> concentration (or 240 vice versa) knowing that:

$$\delta_{O_2/Ar} = \left( \frac{([O_2]/[Ar])_{sample}}{([O_2]/[Ar])_{reference}} - 1 \right) \times 1000$$

[O<sub>2</sub>] and [Ar] are the concentrations of O<sub>2</sub> and Ar respectively and the reference is the present-day atmospheric air.

Before analysis, samples are purified to isolate O<sub>2</sub> and Ar from total air using a gas chromatography 245 column as in Barkan and Luz (2003). Measurements are then performed using a Thermo MAT 253 mass spectrometer (Thermo Scientific) equipped with dual inlet as described in Paul et al. (2023). For each sample, 2 sequences of 16 measurements are performed for measurements of δ<sup>18</sup>O of O<sub>2</sub> with a



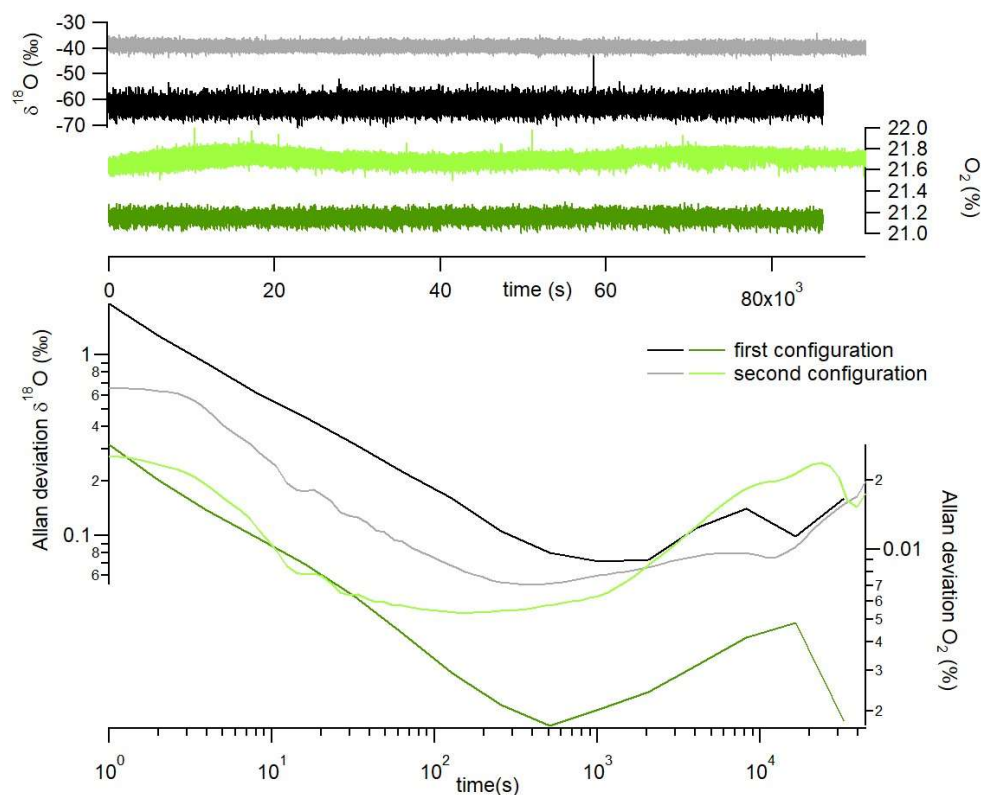
final uncertainty is 0.03 ‰ (1 $\sigma$ ). These sequences are followed by two peak jumping sequences to determine  $\delta\text{O}_2/\text{Ar}$  which is associated with a final uncertainty of 0.5 ‰ (1 $\sigma$ ).

## 250 **3. Results and discussion**

### 3.1 Precision and drift

The instrument was primarily designed and optimized to measure oxygen isotope ratio of dioxygen ( $\delta^{18}\text{O}$  of  $\text{O}_2$ ), but was also capable of measuring, simultaneously, dioxygen concentration.

The first characterization of the instrument was done through the measurement of the Allan deviation  
255 (Figure 2). We introduced in the instrument over several hours dry atmospheric air, which had a constant elemental and isotopic  $\text{O}_2$  composition. Allan deviation was done repeatedly for each different configuration, and the result shown is a typical reproducible result. The minimum of the Allan deviation was reached between 10 and 20 minutes of measurements for both  $\text{O}_2$  concentration and  $\delta^{18}\text{O}$  of  $\text{O}_2$ , and with both configurations (Figure 2). The precision achieved for  $\text{O}_2$  concentration  
260 measurement was better using the initial configuration (0.002 ‰; Figure 2 dark green data) than the second configuration (0.005 ‰; Figure 2 light green data). On the contrary, the  $\delta^{18}\text{O}$  of  $\text{O}_2$  minimal Allan deviation was lower with the second configuration than the initial one (50 ppm vs 80 ppm respectively; Figure 2 grey and dark data).



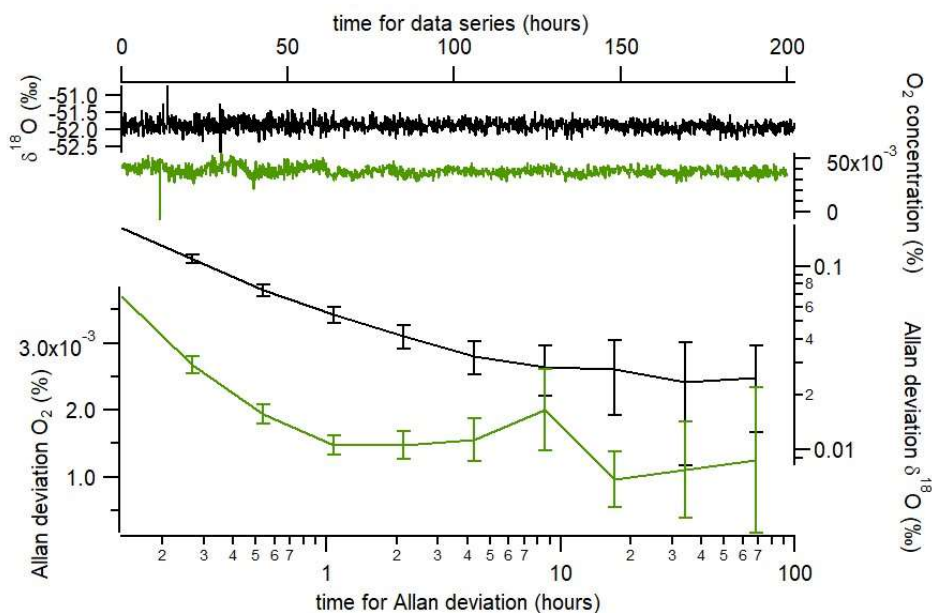
265 Figure 2: Top panel shows continuous measurement of  $\delta^{18}\text{O}$  of  $\text{O}_2$  (grey and black) and  $\text{O}_2$   
concentration (light and dark green). Down panel shows Allan deviation plots based on continuous  
measurement of both  $\delta^{18}\text{O}$  of  $\text{O}_2$  (grey and black) and  $\text{O}_2$  concentration (light and dark green). Black  
and dark green are used for initial configuration; grey and light green for second configuration.

270 After 2 hours, the values of the Allan deviations stayed below 0.2 ‰ for  $\delta^{18}\text{O}$  of  $\text{O}_2$  and 0.03 % for  $\text{O}_2$   
concentration. This showed a moderate drift of the instrument and the need for regular measurement  
of standard during experimentation.

To assess the stability of the instrument on periods longer than 2 hours, we ran measurements of two  
standards during 8 consecutive days. The 2 standards were dry atmospheric air and a mixing of  $\text{O}_2$  and  
275  $\text{N}_2$  in atmospheric proportions (synthetic air from Air Liquide). The evolution of the Allan deviation on



280 Figure 3 was calculated from successive injections of the two standards every 4 minutes. Averages of  $\delta^{18}\text{O}$  of  $\text{O}_2$  and  $\text{O}_2$  concentration were calculated taking into account the 2 last minutes (the first two minutes after injection were removed from the calculation to take into account memory effect). With this approach, we obtained an Allan deviation for  $\delta^{18}\text{O}$  of  $\text{O}_2$  below 0.03 ‰ after 6 hours of measurements. The evolution of  $\text{O}_2$  concentration was marked by a diurnal variability which may have been linked with room temperature changes. The Allan deviation however reached values lower than  $1.5 \cdot 10^{-3} \%$  after 15 hours of measurements.



285 Figure 3: Evolution of difference in mean  $\delta^{18}\text{O}$  of  $\text{O}_2$  and  $\text{O}_2$  concentration when running successive  
290 measurements of two gases (dry atmospheric air and synthetic air) at a periodicity of 8 minutes (4  
minutes of atmospheric air followed by 4 minutes of synthetic air). The data used for calculation are  
the mean values obtained over the last 2 minutes of measurements of each gas. For this series of  
measurements, the initial configuration has been used but a similar result was obtained with the  
second configuration.



### 3.2 Influence of water vapor concentration

We measured the dependence of  $\delta^{18}\text{O}$  of  $\text{O}_2$  and  $\text{O}_2$  concentration on humidity and found that there was only a slight dependence. A dependence of  $\delta^{18}\text{O}$  of  $\text{O}_2$  and  $\text{O}_2$  concentration on humidity is actually  
295 expected for two reasons. First, there is no water vapor absorption line with sufficient intensity to be relevant even at high humidity levels, within the wavelength range analyzed by the instrument. Second, water vapor could still significantly affect the linewidth of all the oxygen lines by collisional broadening. Indeed, even at the modest 1 % mixing ratios corresponding to high atmospheric humidity, water vapor is known to produce significantly enhanced pressure broadening of the  
300 absorption lines of other molecules compared to major atmospheric components like  $\text{N}_2$  or  $\text{O}_2$ . As a consequence, and even if we can correct for the humidity influence, we prefer measuring  $\delta^{18}\text{O}$  of  $\text{O}_2$  and  $\text{O}_2$  concentration after gas have been dried before introduction in the instrument.

### 3.3 Linearity

An influence of  $\text{O}_2$  concentration on  $\delta^{18}\text{O}$  of  $\text{O}_2$  was expected. Indeed, the parameterized models used  
305 for spectrum simulations are associated with uncertainties so that using the theoretical spectroscopic profile does not enable us to faithfully reproduce the shape of the experimental spectrum. As a consequence, we cannot precisely subtract the effect of the amplitude variation of the large  $^{16}\text{O}$  line (directly linked to the abundance of  $\text{O}_2$ ) on the neighboring  $^{18}\text{O}$  line (see spectrum in Figure 1). This difficulty can be overcome by quantifying this effect through the study of the influence of  $\text{O}_2$   
310 concentration on the measured  $\delta^{18}\text{O}$  of  $\text{O}_2$ . Figure 4 showed the linearity effect, *i.e.* the evolution of  $\delta^{18}\text{O}$  of  $\text{O}_2$  with increasing  $\text{O}_2$  concentration. Standard dry atmospheric air enriched with  $\text{O}_2$  was diluted with nitrogen to measure 6 different  $\text{O}_2$  mixing ratios (Figure 4 x-axis). The difference in  $\delta^{18}\text{O}$  of  $\text{O}_2$  between diluted standard and atmospheric air was then used to correct for any instrument drift (Figure 4 y-axis). The influence of  $\text{O}_2$  concentration on  $\delta^{18}\text{O}$  of  $\text{O}_2$  was clearly significant.  $\delta^{18}\text{O}$  of  $\text{O}_2$   
315 increased by 0.37 ‰ with 1 % increase in  $\text{O}_2$  concentration (Figure 4).

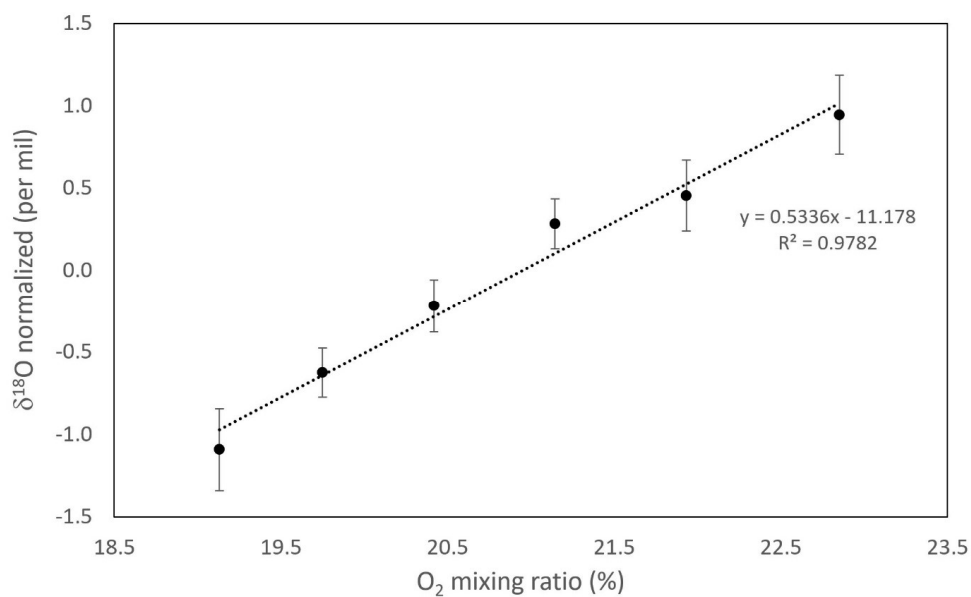


Figure 4: Evolution of the difference in  $\delta^{18}\text{O}$  of  $\text{O}_2$  between a diluted standard (atmospheric air enriched with  $\text{O}_2$ ) with  $\text{N}_2$  and the atmospheric air vs  $\text{O}_2$  concentration of the diluted standard.  $\delta^{18}\text{O}$  is normalized for the ambient  $\text{O}_2$  mixing ratio, and error bars are the standard deviation of individual measurements ( $n=27$ ). This result was obtained with the initial configuration.

Finally, note that the spectroscopic profile is influenced by many environmental parameters. Because of possible drift in pressure and temperature sensors, it is a good practice to regularly check the evolution of this influence of  $\text{O}_2$  on the measured  $\delta^{18}\text{O}$  of  $\text{O}_2$  once every 15 days.

### 3.4 Response time

The response time of the analyzer, when switching between different gas streams, was dependent on the total volume of the system (valve, filter, dryer, tubing, and the instrument internal volume) and the flow rate at the inlet. It was determined that 2 minutes purge time, between samples, were necessary to reach a new steady state for both  $\text{O}_2$  concentration and  $\delta^{18}\text{O}$  of  $\text{O}_2$  (Figure 5).

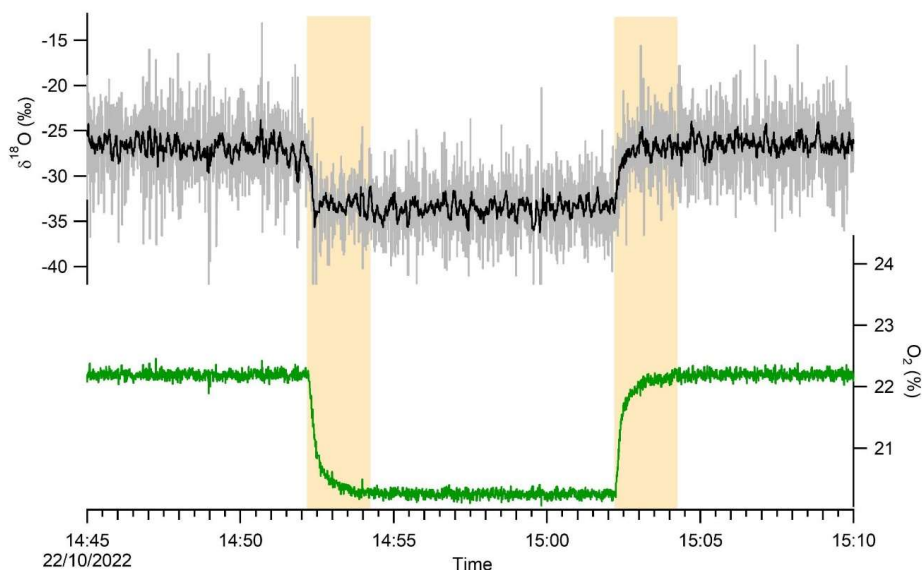


Figure 5: Raw data of  $\delta^{18}\text{O}$  of  $\text{O}_2$  (3 Hz, gray line) and moving average (over 5 second, black line) measured with two gas streams with contrasted  $\text{O}_2$  concentration (green line). The response time is outlined in yellow. These results were exactly the same for the two configurations.

### 3.5 Calibration strategy

Based on the detailed results above, we used the following strategy to ensure good quality measurements of the isotopic and elemental composition of  $\text{O}_2$  in atmospheric air using an OF-CEAS instrument.

1- Place a magnesium perchlorate trap at the entrance of the instrument to work with dry air, hence easily work with standards made of dry air and avoid the dilution effect observed on the  $\text{O}_2$  concentration.

2- According to our observations, we suggest checking the dependency of the  $\delta^{18}\text{O}$  of  $\text{O}_2$  on  $\text{O}_2$  concentration by running successive dilution of a standard with  $\text{N}_2$  every 15 days.



3- A two-point calibration is needed with different values of  $\delta^{18}\text{O}$  of  $\text{O}_2$  and  $\text{O}_2$  concentration. In our case, we used dry atmospheric air and a standard made of dry atmospheric air enriched with 2 % of  $\text{O}_2$  (hence  $\text{O}_2$  concentration of 23 % instead of 21 % in dry atmospheric air). Our tests have shown that the measured difference in  $\delta^{18}\text{O}$  of  $\text{O}_2$  and in  $\text{O}_2$  concentration between the two standards is stable over a 24 hours period. As a consequence, it is enough to run the two standards only once or twice a day and then to measure only one standard with the measurements in the daily routine.

4- The evolution of the Allan variance suggested that, to avoid any drift, a one-point calibration should be done at least every 20 minutes. Moreover, to obtain a small  $1\sigma$  value, averages over 5-10 minutes should be done for each sample injection.

5- In order to account for the instrument response time, it is important to remove the first 2 minutes from the measurement series (purge time) when we switch from one standard to a sample or from one standard to another standard.

6- Finally, for our purpose, we used the following measurement sequence:

- Every 15 days: calibration of the influence of  $\text{O}_2$  concentration on  $\delta^{18}\text{O}$  of  $\text{O}_2$
- Every morning: 6-minutes measurement of atmospheric air enriched with  $\text{O}_2$  and 6-minutes measurement of atmospheric air. Only the last 4 minutes of each plateau were kept for calculation of the average values.
- During the day: 6-minutes measurements of dry atmospheric air, 6-minutes measurements of sample 1, 6-minutes measurements of sample 2, 6-minutes measurements of sample 3, back to 6-minutes measurement of dry atmospheric air. Only the last 4 minutes of each plateau were kept for calculation of the average values.

### 3.6 Accuracy of measurements: comparison with IRMS measurements

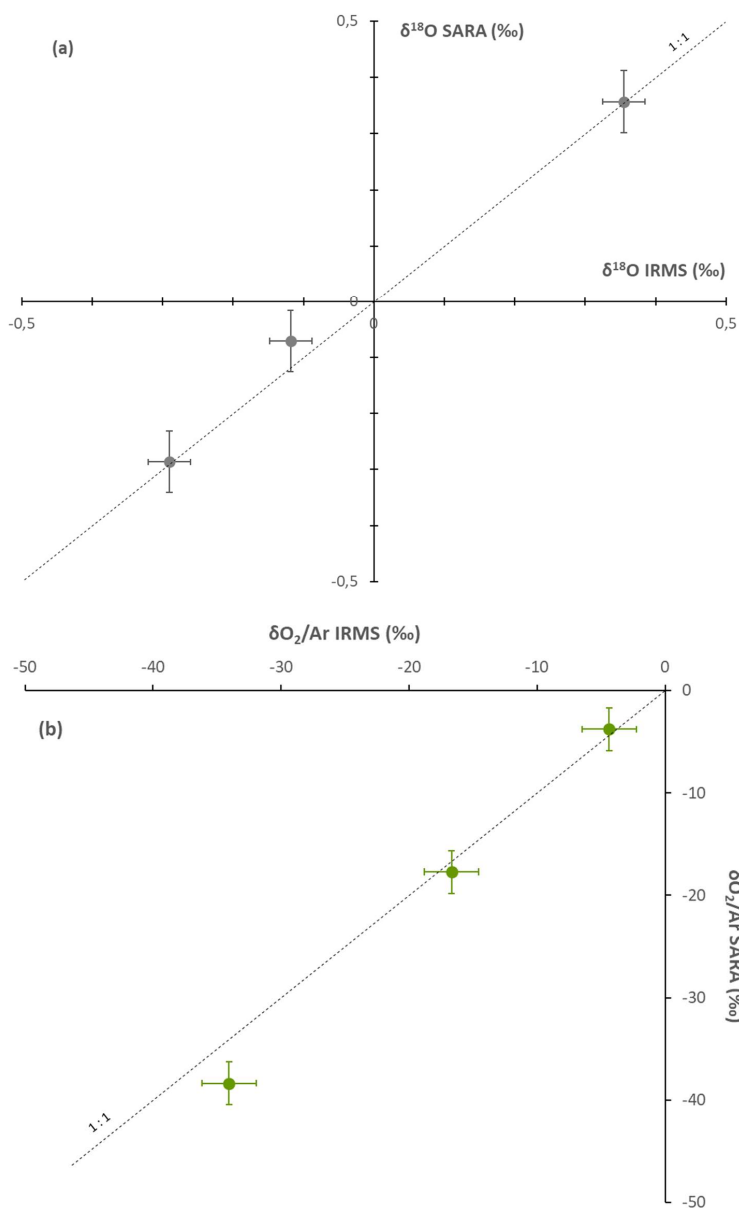
In order to validate the performance of this new analyzer, with the calibration sequence proposed in the previous section, we measured the same samples with our analyzer and with an IRMS. We sampled air in 5 mL flasks from a closed biological chamber while the analyzer was measuring the elemental and isotopic composition of  $\text{O}_2$  following the sequence described above. We measured the isotopic





value of O<sub>2</sub> from the flasks by IRMS (see section 2.3). These values were compared to the values obtained by the analyzer during the same period.

375 The results of this comparison are displayed on Figure 6 for configuration 1 (same result was obtained for configuration 2). The values obtained by the two techniques agree for the 3 biological samples within uncertainty range for measurements of  $\delta^{18}\text{O}$  of O<sub>2</sub>, and with only a slight discrepancy for O<sub>2</sub> concentration, which validates the use of the spectroscopy analyzer for ambient air and biological chambers measurements.



380

Figure 6: Comparison of the concentration (a) and isotopic composition (b) of  $\text{O}_2$  obtained by IRMS and by our spectroscopic analyzer (SARA) for different biological samples. The dashed line shows the 1:1 relationship between  $\delta^{18}\text{O}$  measured by IRMS and  $\delta^{18}\text{O}$  measured by the spectroscopic analyzer.



#### **4. Conclusion**

385 We developed a new instrument based on OF-CEAS technique enabling continuous measurements of  
elemental and isotopic composition of O<sub>2</sub> in the atmosphere. We targeted the region of the dioxygen  
absorption band around 760 nm to capture a signal for <sup>16</sup>O-<sup>17</sup>O, <sup>16</sup>O-<sup>16</sup>O and <sup>18</sup>O-<sup>18</sup>O and developed a  
special fitting for the <sup>16</sup>O-<sup>16</sup>O peak which is saturated.

The instrument has been characterized and we could reach a precision of 0.002 % on O<sub>2</sub> concentration  
390 and 50 ppm on δ<sup>18</sup>O of O<sub>2</sub> for an integration time of 10 minutes. The drift of the instrument  
deteriorates the signal but the values for Allan deviations stay below 0.2 ‰ for δ<sup>18</sup>O of O<sub>2</sub> and 0.03 %  
for O<sub>2</sub> concentration after 2 hours of continuous measurement. The measurements are not affected  
by humidity in the atmosphere but O<sub>2</sub> concentration has an influence on δ<sup>18</sup>O of O<sub>2</sub> which should  
hence be quantified.

395 Based on the performances of the instrument, we proposed a procedure for running O<sub>2</sub> measurements  
for sample or in a continuous way based on a frequent (every 20 minutes) injection of calibration  
standard. This procedure permitted to obtain performance in good agreement with dual inlet IRMS  
measurements in a shorter time. It was particularly adapted for monitoring biological processes in a  
continuous way.

400 In the future, this instrument may be used in several set-ups where a continuous measurement of O<sub>2</sub>  
concentration and δ<sup>18</sup>O of O<sub>2</sub> is needed. The instrument was also able to measure the δ<sup>17</sup>O of O<sub>2</sub> but  
the current precision was not sufficient yet for competing with IRMS measurements.

#### **Data availability**

405 The data supporting the conclusions of this paper is available upon request.

#### **Author contributions**

AL and CPi designed the project. DR designed the optical spectrometer, with assistance and expertise  
from MF and KJ, and most of the hardware was purchased to KJ from AP2E. MF conducted the initial  
410 tests and tuning at LiPhy. Final tuning was performed at Liphy by DR and JC. CPi, JS, CPa carried out  
the experiments at ECOTRON of Montpellier and FP, NB and TL at LSCE. CPi, JS, CPa, NB and AL



analyzed the data from the optical spectrometer and CPa and AL analyzed the data from IRMS. CPI, DR, JS and AL prepared the manuscript with contributions from all the authors.

#### 415 Competing interests

The authors declare that they have no conflict of interest.

#### Acknowledgements

The research leading to these results has received funding from the European Research Council under the European Union H2020 Programme (H2020/20192024)/ERC grant agreement no. 817493 (ERC  
420 ICORDA). The authors acknowledge the scientific and technical support of PANOPLY (Plateforme ANalytique géOsciences Paris-saclaY), Paris-Saclay University, France. This study benefited from the CNRS resources allocated to the French ECOTRONS Research Infrastructure, from the Occitanie Region and FEDER investments as well as from the state allocation 'Investissement d'Avenir' AnaEE- France ANR-11-INBS-0001. We would also like to thank Sébastien Devidal, Abdelaziz Faez, Olivier Ravel and  
425 Alex Milcu from ECOTRON of Montpellier for their help.

#### Bibliography

- Barkan, E. and Luz, B.: High-precision measurements of  $^{17}\text{O}/^{16}\text{O}$  and  $^{18}\text{O}/^{16}\text{O}$  of  $\text{O}_2$  and  $\text{O}_2/\text{Ar}$  ratio in air, *Rapid Commun. Mass Spectrom.*, 17, 2809–2814, <https://doi.org/10.1002/rcm.1267>, 2003.
- 430 Bender, M., Sowers, T., and Labeyrie, L.: The Dole Effect and its variations during the last 130,000 years as measured in the Vostok Ice Core, *Glob. Biogeochem. Cycles*, 8, 363–376, <https://doi.org/10.1029/94GB00724>, 1994.
- Berhanu, T. A., Hoffnagle, J., Rella, C., Kimhak, D., Nyfeler, P., and Leuenberger, M.: High-precision atmospheric oxygen measurement comparisons between a newly built CRDS analyzer and existing measurement techniques, *Atmospheric Meas. Tech.*, 12, 6803–6826, <https://doi.org/10.5194/amt-12-6803-2019>, 2019.
- 435 Brandon, M., Landais, A., Duchamp-Alphonse, S., Favre, V., Schmitz, L., Abrial, H., Prié, F., Extier, T., and Blunier, T.: Exceptionally high biosphere productivity at the beginning of Marine Isotopic Stage 11, *Nat. Commun.*, 11, 2112, <https://doi.org/10.1038/s41467-020-15739-2>, 2020.
- 440 Extier, T., Landais, A., Bréant, C., Prié, F., Bazin, L., Dreyfus, G., Roche, D. M., and Leuenberger, M.: On the use of  $\delta^{18}\text{O}_{\text{atm}}$  for ice core dating, *Quat. Sci. Rev.*, 185, 244–257, <https://doi.org/10.1016/j.quascirev.2018.02.008>, 2018.



- 445 Goto, D., Morimoto, S., Ishidoya, S., Ogi, A., Aoki, S., and Nakazawa, T.: Development of a High Precision Continuous Measurement System for the Atmospheric O<sub>2</sub>/N<sub>2</sub> Ratio and Its Application at Aobayama, Sendai, Japan, *J. Meteorol. Soc. Jpn. Ser II*, 91, 179–192, <https://doi.org/10.2151/jmsj.2013-206>, 2013.
- Goto, D., Morimoto, S., Aoki, S., Patra, P. K., and Nakazawa, T.: Seasonal and short-term variations in atmospheric potential oxygen at Ny-Ålesund, Svalbard, *Tellus B Chem. Phys. Meteorol.*, 69, 1311767, <https://doi.org/10.1080/16000889.2017.1311767>, 2017.
- 450 Guy, R. D., Fogel, M. L., and Berry, J. A.: Photosynthetic Fractionation of the Stable Isotopes of Oxygen and Carbon, *Plant Physiol.*, 101, 37–47, <https://doi.org/10.1104/pp.101.1.37>, 1993.
- Helman, Y., Barkan, E., Eisenstadt, D., Luz, B., and Kaplan, A.: Fractionation of the Three Stable Oxygen Isotopes by Oxygen-Producing and Oxygen-Consuming Reactions in Photosynthetic Organisms, *Plant Physiol.*, 138, 2292–2298, <https://doi.org/10.1104/pp.105.063768>, 2005.
- 455 Keeling, R. F. and Manning, A. C.: Studies of Recent Changes in Atmospheric O<sub>2</sub> Content, in: *Treatise on Geochemistry*, Elsevier, 385–404, <https://doi.org/10.1016/B978-0-08-095975-7.00420-4>, 2014.
- Keeling, R. F. and Shertz, S. R.: Seasonal and interannual variations in atmospheric oxygen and implications for the global carbon cycle, *Nature*, 358, 723–727, <https://doi.org/10.1038/358723a0>, 1992.
- 460 Kerstel, E. and Gianfrani, L.: Advances in laser-based isotope ratio measurements: selected applications, *Appl. Phys. B*, 92, 439–449, <https://doi.org/10.1007/s00340-008-3128-x>, 2008.
- Landais, A., Dreyfus, G., Capron, E., Masson-Delmotte, V., Sanchez-Goñi, M. F., Desprat, S., Hoffmann, G., Jouzel, J., Leuenberger, M., and Johnsen, S.: What drives the millennial and orbital variations of δ<sup>18</sup>O<sub>atm</sub>?, *Quat. Sci. Rev.*, 29, 235–246, <https://doi.org/10.1016/j.quascirev.2009.07.005>, 2010.
- 465 Landsberg, J., Romanini, D., and Kerstel, E.: Very high finesse optical-feedback cavity-enhanced absorption spectrometer for low concentration water vapor isotope analyses, *Opt Lett*, 39, 1795–1798, <https://doi.org/10.1364/OL.39.001795>, 2014.
- 470 Lechevallier, L., Grilli, R., Kerstel, E., Romanini, D., and Chappellaz, J.: Simultaneous detection of C<sub>2</sub>H<sub>6</sub>, CH<sub>4</sub>, and δ<sup>13</sup>C-CH<sub>4</sub> using optical feedback cavity-enhanced absorption spectroscopy in the mid-infrared region: towards application for dissolved gas measurements, *Atmospheric Meas. Tech.*, 12, 3101–3109, <https://doi.org/10.5194/amt-12-3101-2019>, 2019.
- 475 Leroy-Dos Santos, C., Casado, M., Prié, F., Jossoud, O., Kerstel, E., Farradèche, M., Kassi, S., Fourré, E., and Landais, A.: A dedicated robust instrument for water vapor generation at low humidity for use with a laser water isotope analyzer in cold and dry polar regions, *Atmospheric Meas. Tech.*, 14, 2907–2918, <https://doi.org/10.5194/amt-14-2907-2021>, 2021.
- Luz, B. and Barkan, E.: Assessment of Oceanic Productivity with the Triple-Isotope Composition of Dissolved Oxygen, *Science*, 288, 2028–2031, <https://doi.org/10.1126/science.288.5473.2028>, 2000.
- 480 Luz, B. and Barkan, E.: The isotopic composition of atmospheric oxygen, *Glob. Biogeochem. Cycles*, 25, 1–14, <https://doi.org/10.1029/2010GB003883>, 2011.



- Luz, B., Barkan, E., Bender, M. L., Thiemens, M. H., and Boering, K. A.: Triple-isotope composition of atmospheric oxygen as a tracer of biosphere productivity, *Nature*, 400, 547–550, <https://doi.org/10.1038/22987>, 1999.
- 485 Morville, J., Kassi, S., Chenevier, M., and Romanini, D.: Fast, low-noise, mode-by-mode, cavity-enhanced absorption spectroscopy by diode-laser self-locking, *Appl. Phys. B*, 80, 1027–1038, <https://doi.org/10.1007/s00340-005-1828-z>, 2005.
- Morville, J., Romanini, D., and Kerstel, E.: Cavity Enhanced Absorption Spectroscopy with Optical Feedback, in: *Cavity-Enhanced Spectroscopy and Sensing*, vol. 179, edited by: Gagliardi, G. and Loock, H.-P., Springer Berlin Heidelberg, Berlin, Heidelberg, 163–209, [https://doi.org/10.1007/978-3-642-40003-2\\_5](https://doi.org/10.1007/978-3-642-40003-2_5), 2014.
- 490 Paul, C., Piel, C., Sauze, J., Pasquier, N., Prié, F., Devidal, S., Jacob, R., Dapoigny, A., Jossoud, O., Milcu, A., and Landais, A.: Determination of respiration and photosynthesis fractionation factors for atmospheric dioxygen inferred from a vegetation–soil–atmosphere analogue of the terrestrial biosphere in closed chambers, *Biogeosciences*, 20, 1047–1062, <https://doi.org/10.5194/bg-20-1047-2023>, 2023.
- 495 Severinghaus, J. P., Beaudette, R., Headly, M. A., Taylor, K., and Brook, E. J.: Oxygen-18 of O<sub>2</sub> Records the Impact of Abrupt Climate Change on the Terrestrial Biosphere, *Science*, 324, 1431–1434, <https://doi.org/10.1126/science.1169473>, 2009.
- 500 Stephens, B. B., Keeling, R. F., Heimann, M., Six, K. D., Murnane, R., and Caldeira, K.: Testing global ocean carbon cycle models using measurements of atmospheric O<sub>2</sub> and CO<sub>2</sub> concentration, *Glob. Biogeochem. Cycles*, 12, 213–230, <https://doi.org/10.1029/97GB03500>, 1998.
- Stolper, D. A., Bender, M. L., Dreyfus, G. B., Yan, Y., and Higgins, J. A.: A Pleistocene ice core record of atmospheric O<sub>2</sub> concentrations, *Science*, 353, 1427–1430, <https://doi.org/10.1126/science.aaf5445>, 2016.
- 505 Stolper, D. A., Fischer, W. W., and Bender, M. L.: Effects of temperature and carbon source on the isotopic fractionations associated with O<sub>2</sub> respiration for 17O/16O and 18O/16O ratios in *E. coli*, *Geochim. Cosmochim. Acta*, 240, 152–172, <https://doi.org/10.1016/j.gca.2018.07.039>, 2018.
- Tohjima, Y.: Method for measuring changes in the atmospheric O<sub>2</sub>/N<sub>2</sub> ratio by a gas chromatograph equipped with a thermal conductivity detector, *J. Geophys. Res. Atmospheres*, 105, 14575–14584, <https://doi.org/10.1029/2000JD900057>, 2000.
- 510 Yang, J.-W., Brandon, M., Landais, A., Duchamp-Alphonse, S., Blunier, T., Prié, F., and Extier, T.: Global biosphere primary productivity changes during the past eight glacial cycles, *Science*, 375, 1145–1151, <https://doi.org/10.1126/science.abj8826>, 2022.